Nonlinear analysis of interior and exterior beam-column connections under reversed cyclic loading

Nonlinear analysis of interior and exterior beam-column connections under reversed cyclic loading

A Tambusay[1,2], B Suryanto[1*], P Suprobo[2], JJM Nelson[1]

[1]Institute for Sustainable Built Environment, School of Energy, Geoscience, Infrastructure and Society, Heriot-Watt University, Edinburgh, United Kingdom.
[2]Department of Civil Engineering, Faculty of Civil, Planning and Geo Engineering, Sepuluh Nopember Institute of Technology, Surabaya, East Java, Indonesia.

*Corresponding author's e-mail: B.Suryanto@hw.ac.uk

Abstract. This paper presents a case study into the application of nonlinear finite element for the analysis of interior and exterior beam-column joints under reversed cyclic loading. Three beam-column joints, with different reinforcement configurations and test conditions, were considered to assess the accuracy of the currently available constitutive models in predicting the full hysteretic response of beam-column joints under reversed cyclic loading. To this end, the three beam-column joints were modelled in ATENA-GiD which implements nonlinear constitutive models for steel and concrete, the latter of which are formulated within the context of crack-band and crush-band approaches. In this paper, the default constitutive models in the program were employed to evaluate the accuracy of the existing modelling and analysis procedures. From the series of results presented, it is shown that the existing constitutive models are capable of predicting various aspects of the joint behaviour under reversed cyclic loading with good accuracy. This includes the peak load capacity, degrees of pinching and strength degradation, strength and stiffness degradation, unloading and reloading stiffnesses, crack patterns and failure modes.

Keywords: ATENA; beam-column joint; crack pattern; cyclic loading; exterior joint; finite element analysis; hysteresis loop; interior joint.

1. Introduction

The seismic performance of reinforced concrete, moment-resisting frame structures has long been an important subject for researchers and practising engineers, in particular the performance of the beam-column connections due to their critical role in providing continuity among the structural elements in a reinforced concrete frame structure [1,2]. The behaviour of beam-column connections with various designs and detailing has been extensively studied for decades, providing a knowledge base that forms the basis of the modern seismic design provisions [3,4]. Despite the adoption of such design provisions in current practice, damage from recent earthquakes has shown that joint cracking and failure are still commonplace and have been cited repeatedly in post-earthquake reconnaissance reports as a primary contributing factor that is responsible for the partial or full collapse of a building. This is shown, for example, in the partial collapse of the Kaiser Permanente building in Granada Hills during the 1994 Northridge earthquake [5] and the devastating failure of several multi-story buildings in Turkey during the 1999 Kocaeli (Izmit) earthquake [6,7]. In many instances, the issue can be linked to joint shear distress and poor detailing in the joint regions, including inadequate confining

reinforcement and insufficient anchorage lengths. This has certainly added to the known deficiency of beam-column joints, which is characterised by poor hysteresis response and energy dissipation.

Considering the poor hysteresis response of beam-column joints, many modern design codes have adopted the capacity design principle [3,4] to protect joints from undergoing significant distress. This is achieved by creating sacrificial regions, typically in the beam ends, known as plastic hinges. Generally, these regions need to be designed with specific reinforcement configurations so that they can undergo large inelastic deformation and hence produce a highly ductile response under seismic loading. Detailing of reinforcing bars plays a critical role in this regard as these regions must be able to develop significant inelastic flexural action without compromising structural integrity [8,9].

Although most modern reinforced concrete buildings located in seismic regions have been designed following the modern seismic design code provisions, many existing structures, particularly those designed to older design codes or those constructed, are in need of assessment of their seismic performance. The availability of nonlinear finite element analysis programmes can be useful in this regard as it allows for the analysis of complex problems to a high degree of accuracy. It is of the authors' opinion that, with the exponential growth of computing power, detailed structural appraisals incorporating computational modelling are worth pursuing.

In this paper, the application of three-dimensional nonlinear finite element analysis is demonstrated to cement the value of computational modelling in providing a detailed assessment of the response of beam-column joints under reversed cyclic loading. Experimental data was taken from three different groups of researchers [10,11,12] to assess the objectivity of nonlinear finite element modelling when applied to different specimen, materials, boundary and load conditions. A combination of plasticity and fracture models in conjunction with a fixed crack model and crack-band approach was adopted to this end.

2. Details of Beam-Column Connections

Two interior and one exterior beam-column specimens were considered for the analysis. This includes one of the interior beam-column joints tested by Fuji and Morita [10], one interior joint tested by Shiohara and Kusuhara [11], and another exterior joint recently tested by the authors [12]. The details of each specimen are presented below and summarised in Table 1.

In 1991, Fuji and Morita undertook a comprehensive experimental programme involving the testing of four pairs of one-third scale interior and exterior joints [10]. The main purpose of the experiment was to investigate the effects of varying levels of column axial load and the amount of joint hoop reinforcement on the shear capacity of the joint. All specimens were designed to allow for the joint region to develop varying levels of distress prior to the formation of flexural hinging in the adjoining beam and column. In this work, specimen A1 (hereafter referred to as FM/A1), which comprised a 1.5m long column and a 2.0m long beam, was selected. Figure 1 displays the cross-sections and bar detailing used in the specimen. The beam had a cross-section of 160 by 250 mm and was reinforced with eight D10 high-strength longitudinal bars (provided in two layers) near the top and bottom faces of the cross-section. The column had a typical square section of 220 by 220 mm and was reinforced with sixteen D13 longitudinal bars. Closed stirrups with a diameter of 6mm were provided throughout the beams, columns, and joints at a constant spacing of 40 mm.

The second beam-column joint analysed in this paper was from the experimental testing undertaken by Shiohara and Kusuhara in 2001 [11]. The main objective of the experiment was to provide a benchmark against which mathematical models could be validated. Due to the quality and comprehensive documentation of the experiment, this series of test data has been referred to by different researchers for performing validation studies with varying degrees of success [13,14,15]. In this paper, the response of specimen A1 (hereafter referred to as SK/A1) was simulated using a more established modelling strategy than in our recent study [15]. Figure 2 displays the cross-sections and reinforcement details of specimen SK/A1. The specimen comprised a 1.4m long square column and 2.7m long square beam. All columns and beams had the same cross-section of 300 by 300 mm and were reinforced with eight D13 longitudinal bars in the beam and sixteen D13 longitudinal bars in the column. 6mm shear links were provided in the beams, columns, and joints at a spacing of 50 mm.

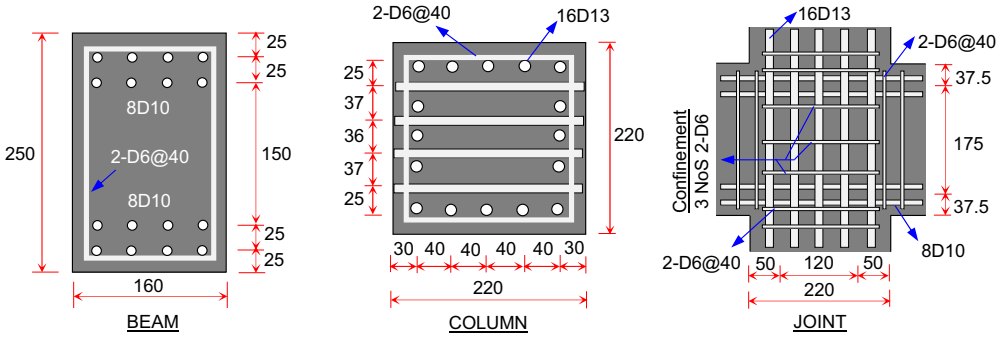

Figure 1. Schematic cross-section dimensions and bar layouts in specimen FM/A1 (adapted from [10]).

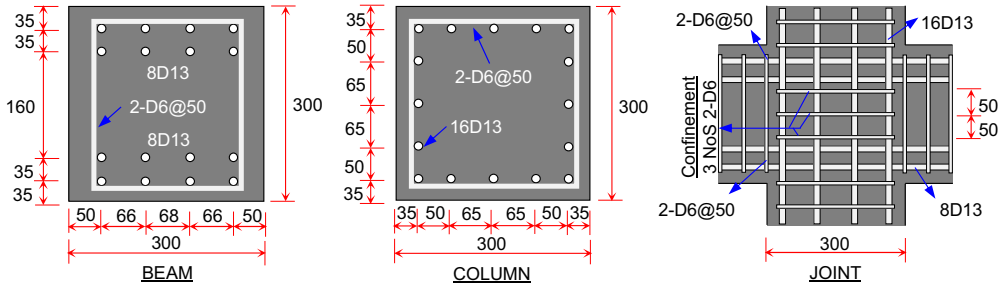

Figure 2. Schematic cross-section dimensions and bar layouts in specimen SK/A1 (adapted from [11]).

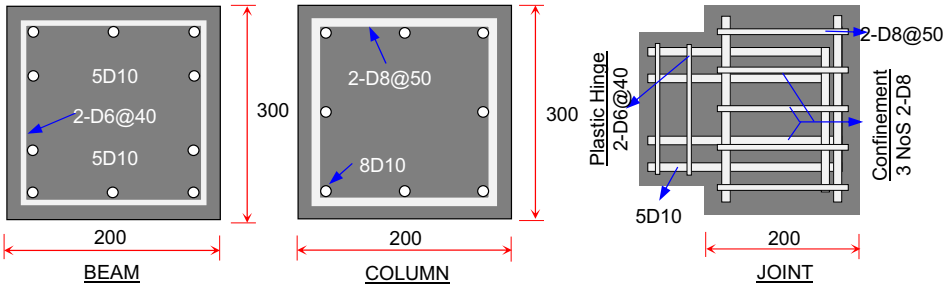

Figure 3. Schematic cross-section dimensions and bar layouts in specimen HW/RC025d (adapted from [12]).

The third beam-column joint referred to in this paper was the half-scale exterior joint tested by the authors [12]. The primary objective of the test programme was to compare the seismic performance of different types of concrete. In this paper, only the exterior joint constructed with ordinary concrete (hereafter referred to as HW/RC025d) was adopted for the reasoning of the similar material with two other counterparts mentioned above. The schematic representation of cross-sections and reinforcement layouts are displayed in Figure 3. The beam-column joint specimen comprised a 1.2m long column and 1.05m long beam. The specimen had a similar square section of 200 by 200 mm and was reinforced with five D10 longitudinal bars which were arranged in two layers on both the top and bottom parts of the beam. In the column, eight D10 longitudinal bars were provided along the full length of the column and were distributed evenly on all four sides of the column. The beam also had 6 mm transverse reinforcement of varying spacings, whereas the column and the joint had 8 mm transverse reinforcement. For further details, the readers are referred to [12].

Table 1. Details of beam-column joint specimens for verification [10,11,12].

Description		FM/A1	SK/A1	HW/RC025d
Model		Interior	Interior	Exterior
Comp. strength of concrete*		40.2 MPa	28.3 MPa	32.9 MPa
Axial Load		147 kN	216 kN	80 kN
Beam(s)	Cross-section	160 × 250 mm	300 × 300 mm	200 × 200 mm
	Span	2260 mm	2700 mm	1030 mm
	Longitudinal bar	8D10 (top and bottom) (1069)#	8D13 (top and bottom) (456)# and (582)&	5D10 (top and bottom) (563)# and (662)&
	Transverse bar	D6 @40 mm (456)#	D6 @50 mm (326)# and (488)&	D6 @40 mm (533)# and (619)&
Columns	Cross-section	220 × 220 mm	300 × 300 mm	200 × 200 mm
	Span	1500 mm	1470 mm	1200 mm
	Longitudinal bar	16D13 (643)#	16D13 (357)# and (493)&	8D10 (563)# and (662)&
	Transverse bar	D6 @40 mm (291)#	D6 @50 mm (326)# and (488)&	D8 @50 mm (581)# and (659)&
Joint	Transverse bar	D6 @40 mm (3 NoS) (291)#	D6 @50 mm (3 NoS) (326)# and (488)&	D8 @40 mm (3 NoS) (581)# and (659)&

Notes:
*Compressive strength on the day of testing
#Yield strength of reinforcing bar (MPa)
&Ultimate strength of reinforcing bar (MPa)

3. Finite Element Analysis

The nonlinear responses of the beam-column joints were performed using a three-dimensional finite element analysis software ATENA Science v5.9.0, developed by Cervenka Consulting [16]. Part of this software includes two fully integrated software packages, GiD and ATENA. GiD is an interactive pre-processor that generates FE models as well as relevant data such as material properties, loading, boundary conditions, and meshes. Additionally, GiD can be used to run an analysis, automatically transferring the FE model and associated data into ATENA Studio, which performs the analysis and provides post-processing capability with real-time visualisation during an analysis [17,18].

The nonlinear constitutive model of concrete used in this study was the default Cementitious2 which was formulated based on the fracture-plastic model and implemented in conjunction with the crack band and crush band approaches [17-20]. In this study, the fixed crack approach was adopted (i.e., the direction of cracking is fixed based on the direction of the principal stresses at the onset of cracking). The direction of principal stresses may rotate during loading and no longer coincide with the crack direction. A brief description of the main constitutive models considered in this paper is presented below. For further details, the readers are referred to [17,21].

Figures 4(a) and (b) display the graphical representation of the constitutive models of concrete used in this study [17,18,22,23]. The Menetrey-Willam plasticity model [24] was used for describing the behaviour of concrete in compression under a multiaxial stress condition. This model comprises nonlinear hardening and linear softening parts. In the hardening model, compressive stresses were computed from the strains in the local coordinate system following the crack orientation [17,18]. Unlike the hardening part, the strain in the softening part was computed based on the displacement following the crush band approach to ensure mesh objectivity [21,25]. The Rankine failure criterion was used for defining concrete cracking. The tensile stress-strain relationship of concrete after cracking was represented with exponential softening function [18,25], with the tensile stress being related to the crack opening displacement and fracture energy following the Hordijk model [26]. In shear, a constant shear factor coefficient (SF), which defines a relationship between normal and shear crack stiffnesses, was used [17,27,28]. The compressive strength reduction was also considered in the modelling to better consider the behaviour of cracked concrete in compression. In this work, the standard concrete softening with a limit reduction factor of 0.8 was considered.

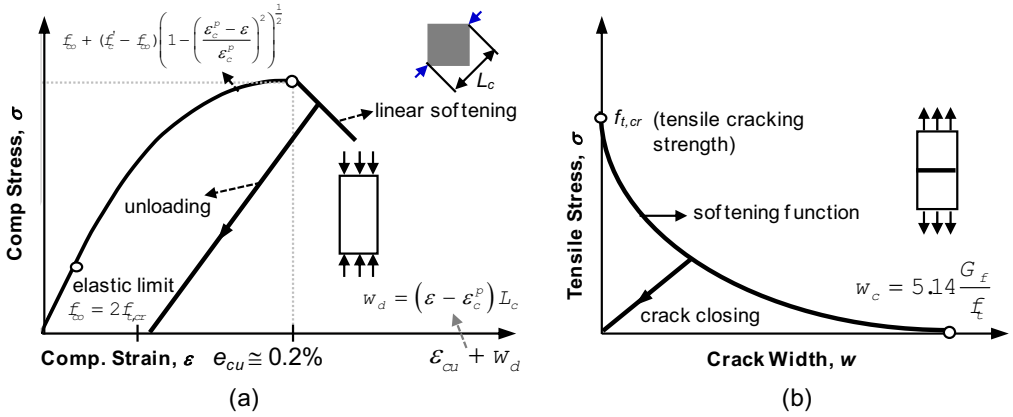

Figure 4. Concrete constitutive model: (a) compression and (b) tension.

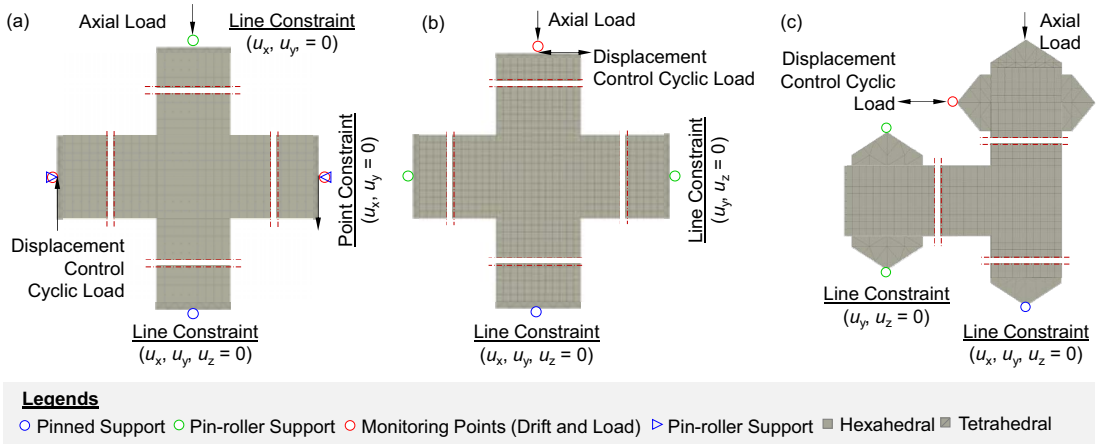

Figure 5. Typical finite element mesh and boundary conditions for beam-column joints: (a) SK/A1; (b) FM/A1; and (c) HW/RC025d. Note that only parts of the models are shown.

Figures 5(a)-(c) display the finite element meshes, boundary conditions, and monitoring points of the three beam-column joints adopted in this study. The concrete was modelled with 8-node hexahedral linear elements with the size of 25 mm for FM/A1 and SK/A1 and 20 mm for HW/RC025d, to maintain the same number of elements (10) across the depth of the members. In FM/A1 and SK/A1, all end plates were modelled using tetrahedral linear elements and were attached to the beam and column end surfaces in the form of end plates, following the actual setup in the experiment. In contrast, the steel plates in HW/RC025d were placed onto the top and bottom surfaces of the column and beams in the form of triangular prism components to simplify the pin and roller supports used in the original experiment. All these plates were assumed to have a linear elastic property to prevent localised yielding.

The embedded reinforcing bars were modelled in discrete representation using 2-node linear truss elements. The material nonlinearity of the bar was computed based on the default bilinear stress-strain relationship with hardening. The elasto-plastic Menegotto-Pinto model [29] was used for the reinforcing bars as it considers Bauschinger's effect throughout unloading and reloading sequences. Bond-slip formulation with geometry type of bar with memory bond was also considered following the nonlinear bond-slip formulation in Model Code 1990 [30]. The key input parameters used in the analysis are summarised in Table 2.

Table 2. Summary of material parameters and finite element input parameters.

No	Parameter	Value/Reference
Concrete constitutive model		
1.	Elastic modulus	CEB-FIP Model Code [30]
2.	Tensile strength	CEB-FIP Model Code [30]
3.	Smeared crack model	1 (fixed crack)
4.	Maximum aggregate size	15 mm (FM/A1); 20 mm (SK/A1); and 10 mm (HW/RC025d)
5.	Unloading factor for cyclic loading	0.2
6.	Critical compressive displacement	0.25 mm following the recommendation [18,25]
7.	Limit of compression strength reduction factor due to transverse cracking	0.8
8.	Crush band minimum	The smallest dimension of the member [18,25]
8.	Eccentricity (defining the shape of the failure surface)	0.52
9.	Plastic flow (defining dilatancy of plastic factor)	0
Reinforcement bar model		
10.	Stress-strain relationship	Bilinear with strain hardening
11.	Bond-slip model for cyclic (bar with memory bond)	CEB-FIP Model Code [30]
12.	Cyclic behaviour (Menegotto-Pinto)	R = 20; C1 = 0.925; and C2 = 0.15
Loading procedure and solution parameter		
13.	Loading procedure for axial load	Static (force-controlled)
14.	Loading procedure for cyclic load reversal	Quasi-static (displacement-controlled)
15.	Iteration method for cyclic	Modified Newton-Raphson
16.	Stiffness type	Elastic predictor with conditional break criteria
17.	Iteration limit	100
18.	Solver	PARDISO

In all models, the lower column was restrained in all three translation directions (e.g., a pinned support). In the first loading interval, the top surface of the upper column was loaded with a constant axial load (see Table 1). In the second and subsequent intervals, reversed cyclic lateral loads were then applied by means of displacement control, with an increment rate of 1.0 mm per step, up to the maximum drift specified for each cycle in the experiment. In SK/A1 and HW/RC025d, the cyclic loads were applied in the horizontal direction at the top of the upper column. Unlike these two specimens, the cyclic loads in specimen FM/A1 were induced through two opposite loads at both ends of the beam. For further details with reference to the test setup and loading protocol, the readers are referred to the original experiments [10,11,12].

In this study, solutions parameters adopted the modified Newton-Raphson iterative solution with the elastic predictor to allow for consistent and easy convergence at each load step. Conditional break criteria were also preferred over the line-searched method, the values of which were set ten times the default values to improve computational stability, particularly when convergence difficulties are encountered. The convergence tolerance was set constant throughout intervals with a value of 1.0% for displacement, residual, and absolute residual error, whilst energy error was set at 0.1%.

4. Results and Discussion

4.1. Comparison of hysteresis response

Figures 6(a)-(c) compare the predicted and observed load-drift responses for all three specimens modelled in this study, with the summary of peak loads for each specimen presented in Table 3. In general terms, there is an excellent agreement between the predicted and observed responses in terms of the shape of the hysteresis loops, initial stiffness, strength and stiffness degradation, and load capacity. A more detailed comparison of the full hysteresis response and failure crack pattern of each specimen is provided below.

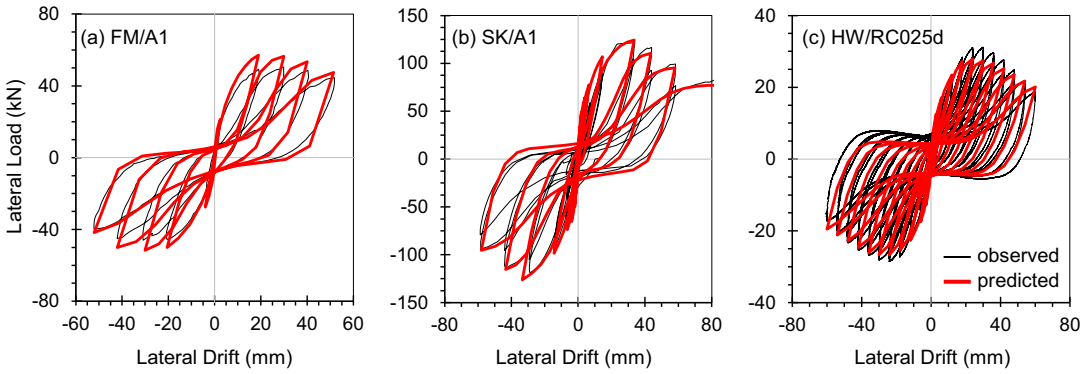

Figure 6. Comparisons of predicted and observed hysteresis response of beam-column joints.

Table 3. Summary of experimental and predicted load capacities.

Beam-column joint model	Positive Loading Direction			Negative Loading Direction		
	$P_{u\text{-}Test}$ (kN)	$P_{u\text{-}Calc}$ (kN)	$P_{u\text{-}Test}/P_{u\text{-}Calc}$ (-)	$P_{u\text{-}Test}$ (kN)	$P_{u\text{-}Calc}$ (kN)	$P_{u\text{-}Test}/P_{u\text{-}Calc}$ (-)
FM/A1	50.43	57.14	0.88	-46.01	-51.56	0.89
SK/A1	121.59	124.43	0.98	-118.56	-126.28	0.94
HW/RC025d	31.15	27.93	1.12	-28.54	-26.68	1.07
		Mean	0.99		Mean	0.97
		CoV (%)	12.13		CoV (%)	9.61

With regard to the response of interior beam-column joint FM/A1, it is evident from Figure 6(a) that the overall hysteresis response predicted by ATENA correlates well with the response observed experimentally, particularly in terms of the response at the initial stages of loading and the decay in strength beyond the peak load. The prediction tends to overestimate the post-cracking stiffness and overall strength in both positive and negative loading directions. This does not however render the accuracy of the adopted material models and finite element procedures in predicting the complete hysteresis response of the beam-column sub-assemblage under reversed cyclic loading. As shown in Table 3, the ratio of the experimental-to-predicted load capacity in the positive and negative loading directions are 0.88 and 0.89, respectively, which is within the acceptable range of accuracy.

Figure 6(b) displays the predicted and observed hysteresis response of interior beam-column joint SK/A1. It is of interest to note that in the original study [11], the hysteresis response of specimen SK/A1 was corrected for the P-delta effects; in this paper, however, the effects of P-delta were reinstated to facilitate direct comparison with the ATENA prediction, which automatically takes the P-delta effects into consideration. As can be seen from Figure 6(b), there is an excellent agreement between the predicted and observed hysteresis response in both the positive and negative loading directions in terms of all aspects of response, including strength, stiffness, ductility, and residual drift. All of which represent a significant improvement to the authors' recent study [15]. Of particular interest are the successful representation of the highly pinched hysteretic response at higher lateral drift levels and the strength and stiffness degradation throughout the entire load cycles, even during the last load cycle which goes beyond 60 mm drift. The ratio of the experimental-to-predicted load capacity in the positive and negative loading directions are 0.98 and 0.94, respectively (Table 3), highlighting once again the accuracy of the finite element models and procedure adopted in this study.

Figure 6(c) presents the observed hysteresis response of exterior beam-column joint HW/RC025d overlaid with the predicted hysteresis data (in red). Overall, there is a reasonable agreement between the predicted and observed responses, particularly in terms of the shape of hysteresis loops, overall strength and stiffness, degrees of stiffness degradation and pinching at each cycle, and the post-peak cyclic deterioration. As summarised in Table 3, the ratios of the experimental-to-predicted strength are 1.12 and 1.07 in respective positive and negative loading directions, which is satisfactory.

4.2. Comparison of crack patterns

To provide further evidence regarding the accuracy of the finite element models and procedure employed in this study, Figures 7 to 9 display the observed crack patterns at failure along with the maximum principal tensile strain plots at the corresponding drift overlaid with the predicted crack patterns. In general, there is a reasonably good agreement between the predicted and experimentally observed failure crack patterns in terms of the extent and location of damage accumulation in the joint core and at the column interface. This signifies accurate predictions of mode of failure and internal load-carrying mechanisms that lead to the failure.

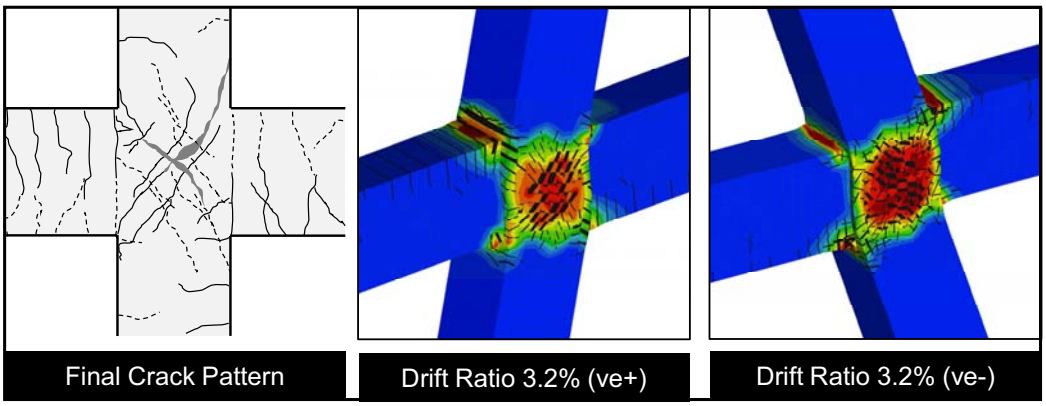

Figure 7. Observed and predicted failure crack patterns of specimen FM/A1.

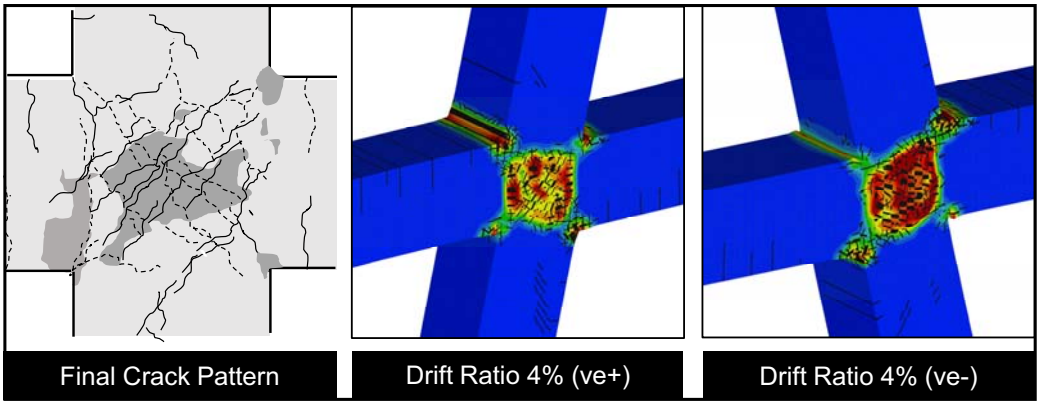

Figure 8. Observed and predicted failure crack patterns of specimen SK/A1.

Concerning the failure crack patterns of specimens FM/A1 and SK/A1, a build-up of damage is evident in the joint core region of both specimens, as indicated by the development of X-shaped cracking throughout the region (see Figures 8). Severe spalling of concrete can also be observed in the joint region, particularly in specimen SK/A1 due to a considerable progression of damage during the last few cycles of loading, which was also reported in the experiment. In specimen SK/A1, the accumulation of damage can also be found at the four corners of the joint, with some clustering of damage apparent over the top and bottom corners of the beam. In this region, considerable residual strain developments could be observed when loaded in the reversed direction, indicating that the beams have developed significant plasticity. The distress in the joint regions of both specimens might be attributed to the marginal overstrength factor for the column as well as the lack of joint confinement. Therefore, it is not surprising that the joint core shows signs of heavy shear distress, followed by diagonal concrete crushing.

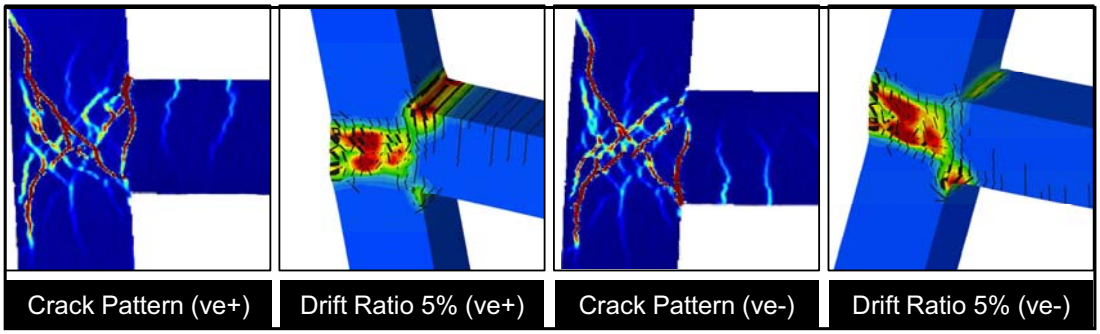

Figure 9. Observed and predicted failure crack patterns of HW/RC-025d.

Figure 9 compares the strain maps obtained from the surface of HW/RC025d at 5% drift in the positive and negative directions (obtained using the digital image correlation (DIC) technique [12,31]) with the predicted crack patterns at the same drift level from the ATENA analysis. It should be noted that the high-contrast lines that appear on the DIC strain maps are representative of individual (discrete) crack formation, while the strain maps obtained from the finite element analysis are a smeared representation of concrete cracking (hence would be expected to be more dispersed in nature). In general terms, there is a reasonably good agreement between the observed and predicted crack patterns. This includes the development of high strain levels at the beam-column interface, which is indicative of a plastic hinge formation, and at the joint core. It is of interest to note that the strain values at the beam-column interface remain high when subjected to reversed loading, which is consistent with the experimental evidence. This would indicate that the beam end must have developed significant plasticity due to the yielding and slippage of reinforcement, which prevents full closure of the flexural cracks upon unloading. At 5% drift, damage is shown to have propagated from the joint core into the column end, while the remaining part of the column is predicted to remain elastic due to the high overstrength factor considered for the column (around 2). No existence of concrete crushing was observed.

5. Concluding Remarks

Computer simulations on three reinforced concrete beam-column joints with a range of design and loading conditions were carried out to check the accuracy of the currently available nonlinear constitutive models for concrete and steel in ATENA. Particular attention has been paid with regard to the capability of the models in predicting various aspects of behaviour under reversed cyclic loading. Based on the results presented, the following conclusions are drawn:

1. The currently available nonlinear constitutive models for concrete and steel are shown to provide accurate predictions of the response of three beam-column joints under reversed cyclic loading. A good agreement in peak loads, shape of hysteresis loops, strength and stiffness degradation, unloading and reloading stiffnesses, crack and damage patterns was obtained.
2. The strong correlation between the predicted and experimental results for three joints with different design considerations and loading conditions justifies the objectivity of the modelling procedure and nonlinear constitutive models adopted in the current work.
3. The agreement between the predicted and observed strength was strong, with discrepancies of less than 10%. From the three validation studies presented, it is shown that the ratio of experimental-to-predicted load capacity in the positive and negative loading directions had an overall mean of 0.99 and 0.97 and a CoV of only 12.1% and 9.6% in the respective directions, indicating high accuracy.
4. The predicted crack patterns in the joint and plastic hinge regions of the three specimens are shown to correlate well with the crack patterns observed in the experiments. Both interior joints are predicted to undergo prominent joint distress, while the exterior joint is predicted to also exhibit flexural hinging. These behavioural responses are consistent with the experimental evidence.

Future work is directed toward extending the scope of the current validation study, by incorporating more test data available in the literature, and using this computer simulation tool for vulnerability assessment, and for reviewing a range of retrofit measures.

Acknowledgements
This work was supported by a Newton Fund Impact Scheme grant, ID 624577537, under the Newton Fund and the Ministry of Research, Technology and Higher Education of the Republic of Indonesia partnership. The grant is funded by the UK Department for Business, Energy and Industrial Strategy and the Indonesian Ministry of Education, Culture, Research, and Technology (Grants No. 342/E4.1/AK.04.PT/2021 and No. 084/E5/PG.02.00.PT/2022) and delivered by the British Council.

References
[1] Kim J and LaFave JM 2007 Key influence parameters for the joint shear behaviour of reinforced concrete (RC) beam-column connections. *Eng. Struct.* 29 10 2523-39
[2] Sagbas G, Vecchio FJ, Christopoulos C Computational modelling of the seismic performance of beam-column subassemblies *J. Earthq. Eng.* 15 640-63
[3] ACI Committee 2019 ACI-318-19: Building code requirements for structural concrete and commentary. Farmington Hills: American Concrete Institute
[4] Joint ACI-ASCE Committee 2002 ACI 352R-02: Recommendations for design of beam-column connections in monolithic reinforced concrete structures. Farmington Hills: American Concrete Institute
[5] Mitchell D, DeVall RH, Saatcioglu M, Simpson R, Tinawi R, Tremblay R 1995 Damage to concrete structures due to the 1994 Northridge earthquake *Can. J. Civ. Eng.* 22 361-77
[6] Deaton JB 2013 Nonlinear finite element analysis of reinforced concrete exterior beam-column joints with nonseismic detailing PhD thesis Georgia Institute of Technology.
[7] Sezen H, Whittaker AS, Elwood KJ, Mosalam KM 2003 Performance of reinforced concrete buildings during the August 17, 1999 Kocaeli, Turkey earthquake, and seismic design and construction practise in Turkey *Eng. Struct.* 25 1 103-14
[8] ASCE Committee 2000 FEMA 356: Prestandard and commentary for seismic rehabilitation of buildings Washington DC: Federal Emergency Management Agency
[9] ASCE Committee 2017 ASCE/SEI 41-17: Seismic evaluation and retrofit of existing buildings Virginia: American Society of Civil Engineers
[10] Fujii S and Morita S 1991 Comparison between interior and exterior RC beam-column joint behavior *ACI Spec. Pub.* (SP123-6) 123 6 145-66
[11] Shiohara H and Kusuhara F 2006 Benchmark test for validation of mathematical models for nonlinear and cyclic behavior of R/C beam-column joints Tokyo: The University of Tokyo
[12] Suryanto B, Tambusay A, Suprobo P, Bregoli G, Aitken MW 2022 Seismic performance of exterior beam-column joints constructed with engineered cementitious composite: comparison with ordinary and steel fibre reinforced concrete *Eng. Struct.* 250 113377
[13] Guner S and Vecchio F J 2010 Analysis of shear-critical reinforced concrete plane frame elements under cyclic loading *J. Struct. Eng.* 137 8 834–43
[14] Pan Z, Guner S and Vecchio F J 2017 Modeling of interior beam-column joints for nonlinear analysis of reinforced concrete frames *Eng. Struct.* 142 182–91
[15] Tambusay A, Suryanto B, Suprobo P 2020 Nonlinear finite element analysis of reinforced concrete beamcolumn joints under reversed cyclic loading *IOP Conf. Ser.: Mater. Sci. Eng.* 930 012055
[16] ATENA, Advanced Tool for Engineering Nonlinear Analysis, available at www.cervenka.cz/products/atena/
[17] Cervenka V, Jendele L, Cervenka J 2018 ATENA program documentation–part 1: theory Cervenka Consulting
[18] Tambusay A, Suprobo P, Suryanto B, Don W 2021 Application of nonlinear finite element analysis on shear-critical reinforced concrete beams *J. Eng. Tech. Sci.* 53 4 210408

[19] Don W, Chong K, Aitken M, Tambusay A, Suryanto B, Suprobo P 2020 Influence of link spacing on concrete shear capacity: experimental investigations and finite element studies *IOP Conf. Ser.: Mater. Sci. Eng.* 930 012052
[20] Suryanto B, Nagai K, Maekawa S 2010 Smeared-crack modeling of R/ECC membranes incorporating an explicit shear transfer model *J. Adv. Conc. Techn.* 8 3 315–26
[21] Cervenka J and Papanikolaou VK 2008 Three-dimensional combined fracture–plastic material model for concrete *Int. J. Plast.* 24 12 2192-220
[22] Don W, Suryanto B, Tambusay A, Suprobo P 2022 Forensic assessments of the influence of reinforcement detailing in reinforced concrete half-joints: A nonlinear finite element study *Struct.* 38 689–703
[23] Chong K, Suryanto B, Tambusay A, Suprobo P 2022 Nonlinear analysis of reinforced geopolymer concrete beams *Civ. Eng. Dimens.* 24 1 1–10
[24] Menetrey P and Willam KJ 1995 Triaxial failure criterion for concrete and its generalization *ACI Struct. J.* 92 3 311–318
[25] Cervenka J, Cervenka V, Laserna S 2018 On crack band model in finite element analysis of concrete fracture in engineering practice *Eng. Fract. Mech.* 197 27–47
[26] Hordijk DA 1991 Local approach to fatigue of concrete PhD Thesis Delft University of Technology
[27] Kolmar, W 1986 Beschreibung der kraftuebertragung über risse in nichtlinearen finite-elementberechnungen von stahlbetontragwerken PhD Thesis Darmstadt University of Technology
[28] Vecchio FJ and Collins MP 1986 The modified compression-field theory for reinforced concrete elements subjected to shear *ACI J.* 83 2 219–31
[29] Menegotto M and Pinto PE 1973 Method of analysis of cyclically loaded RC plane frames including changes in geometry and non-elastic behavior of elements under combined normal force and bending IABSE Symp. (Lisbon: Portugal) 15–22
[30] CEB-FIP Model Code 1990 Comité Euro-International du Béton Inf. Bullet. 195
[31] Tambusay A, Suryanto B, Suprobo P 2020 Digital image correlation for cement-based materials and structural concrete testing *Civ. Eng. Dimens.* 22 1 6–12